SCIENTIA
AGRICOLA

Sombric-like horizon and xanthization in polychrome subtropical soils from Southern Brazil: implications for soil classification

Mariane Chiapini[1] , Jairo Calderari de Oliveira Junior[2] , Judith Schellekens[1] , Jaime Antonio de Almeida[3] , Peter Buurman[4] , Pablo Vidal-Torrado[1]*

[1]Universidade de São Paulo/ESALQ – Depto. de Ciência do Solo, C.P. 09 – 13418-900 – Piracicaba, SP – Brasil.

[2]Universidade Federal do Paraná – Depto. de Ciência do Solo – R. dos Funcionários, 1540 – Curitiba, PR – Brasil.

[3]Universidade do Estado de Santa Catarina – Depto. de Solos e Recursos Naturais – Av. Luis de Camões, 2090 – Lages, SC – Brasil.

[4]Wageningen University and Research/Earth System Science Group, P.O. Box 47 – 6700 AA Wageningen – The Netherlands.

*Corresponding author <pvidal@usp.br>

ABSTRACT: The occurrence of dark subsurface horizons rich in organic matter (OM) associated with polychrome in the B horizon (yellowish over reddish hue) is common in soils from Southern Brazil. The formation of these horizons and the combination with such morphological attributes has not been properly documented, and neither has the cause effect relationship. Four soil profiles with such sombric-like horizons with a yellowish color at the upper part of the B horizon over red subsoil were studied in Southern Brazil. Results from micromorphology, extractable sesquioxide minerals, clay mineralogy and isomorphic substitution of Fe by Al in iron minerals showed that melanization, xanthization, bioturbation, moderate shrinking/swelling and moderate ferralitization were the most evident pedogenetic processes in role. Xanthization is closely related to the sombric-like horizon formation. In the studied area the findings demonstrated that no clay and OM illuviation had taken place. Therefore, the classification of these soils was revisited, so as to take into account the processes that underlie their genesis with emphasis on xanthization, clay illuviation and soil aggregation. The results suggest that the sombric horizon may need redefinition, unless profiles can be found in which illuviation of clay and/or OM can be proven.

Keywords: *Argissolos*, goethite, dark subsurface horizon, shiny peds, matte aggregate faces

Introduction

Sombric and sombric-like horizons are found in well-drained landscape positions with high soil moisture, on high plateaus and/or mountains in tropical and subtropical regions, and several theories exist as to their formation (Almeida et al., 2009; Bockheim, 2012; Almeida et al., 2015). Except for Faivre (1990), sombric horizons described in the literature lack evidence of OM illuviation, and are therefore frequently referred to as sombric-like horizons (De Craene and Laruelle, 1955; Sys et al., 1961; Gouveia et al., 2002; Caner et al., 2003; Almeida et al., 2009; Velasco-Molina et al., 2010). Recently, Chiapini et al. (2018) studied the sombric-like horizons in Southern Brazil from a site that is representative of such conditions. For this area the authors found that the sombric-like horizon is a remnant of an earlier phase of soil formation in which grass vegetation and frequent natural fires caused deep accumulation of black carbon (BC). During subsequent wetter conditions, from the Late Holocene until the present, forest vegetation replaced grass vegetation and fire incidence declined. A similar mechanism may explain the formation of sombric-like horizons in other areas, and was also proposed by Caner et al. (2003).

Taxonomic soil classification systems are based on morphological properties and recognition of key processes responsible for soil genesis (Lebedeva et al, 1999; Bockheim, 2012). Our improved understanding of the formation of the sombric-like horizons from Southern Brazil (Caner et al., 2003; Chiapini et al., 2018), inhibits the correct classification of these soils,

in particular, in the Brazilian Soil Classification System (Embrapa, 2018). Associated with sombric-like horizons in subtropical soils the yellowish color at the upper part of the B horizon over red subsoil can be observed. This process is called xanthization (from the Greek *xanthos*, yellow) (IUSS Working Group WRB, 2015). Xanthization is the conversion of hematite into goethite influenced by constantly moist climatic conditions. In subtropical soils moist conditions and the presence of organic matter inhibit hematite formation or microbial oxidation and are responsible for the preferential reductive dissolution of originally formed hematite turning red soils yellow (Cornell and Schwertmann, 2003). In the present study, the classification of these soils is revisited, taking into account the processes that underlie their formation. The relationship with the formation of the sombric-like horizon and xanthization is highlighted. With this aim in mind, new data of micromorphological, physicochemical, mineralogical and iron and aluminum dissolution analysis were interpreted.

Materials and Methods

Study site

The study area is located in Tijucas do Sul (in the state of Paraná, Brazil; 25°55′41″ S, 49°11′56″ W) (Figure 1). The parent material was described as a colluvium derived from migmatites with local influence of other metamorphic rocks (Santos et al., 2006). The native vegetation was classified as a mixed ombrophylous forest with grassland. The climate is temperate and humid subtropical (Behling et al.,
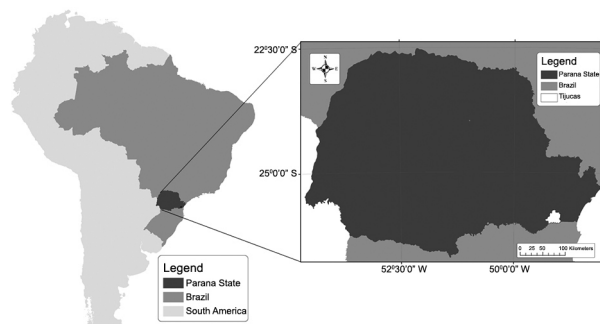
Figure 1 – Location of the study area.

2001). The soils found in the region are classified as *Argissolos*, *Nitossolos*, *Cambissolos* mainly with some local occurrence of *Latossolos* (Embrapa, 2018). The pedologic system is made up of four soil profiles with a sombric-like horizon, previously studied by Chiapini et al. (2018) to assess environmental changes. In this study we used this pedologic system to examine the main soil forming processes in the context of their classification within the three soil classification systems. These included three profiles from a toposequence (P1, P2 and P3) and a profile on the summit of a nearby hill (P4). Figure 2 illustrates a representative profile. Pedogenic horizons were described in the field. Morphological description was based on the field guide elaborated by the FAO (2006). The soil samples were collected according to pedogenic horizon (Table 1). The samples were dried and sieved and the fraction < 2 mm was used for physical (granulometry; Table 2) and chemical analysis (pH_{H2O}, pH_{KCl}, Al^{3+}, $H+Al$; Ca^{2+}, Mg^{2+}, $K+$, total C; base saturation (BS), clay activity and C/N ratio; Table 3) that were presented in Chiapini et al. (2018).

Fe and Al contents

Fe and Al contents were determined from samples of each profile. First, the OM of the soil samples was eliminated by the addition of 30 % H_2O_2 in a water bath. Free Fe and Al oxyhydroxides were extracted by sodium citrate-bicarbonate-dithionite (CBD) treatment (four times at 80 °C for 30 min in a water bath) (Mehra and Jackson, 1960; Jackson, 1979). Amorphous Fe (Fe_o) and Al (Al_o) oxyhydroxides were determined by extraction with 0.2 mol L^{-1} ammonium oxalate in the dark at 3.0 pH (McKeague and Day, 1966). Fe and Al contents were determined by atomic absorption spectrometry. Sodium pyrophosphate (0.1 mol L^{-1}) was extracted at pH 10 according to USDA (1996) providing the Fe and Al that is bound to OM (Fe_p and Al_p) (Table 4).

Mineralogical analysis in the clay fraction

After dispersion with 0.2 mol L^{-1} NaOH, the sand fraction was separated from the silt + clay fractions by sieving (0.053–mm sieve opening), the soil samples (P1: B_3; P2: B_3; P3: B_2 e P4: B_3), after which the clay was separated from the silt by decantation, following Stokes'

Figure 2 – Representative soil profile with sombric-like horizon (P1; Chiapini et al., 2018).

law (Jackson, 1979). Clay samples were saturated with Mg^{2+} (Mg 25 °C) and solvated with ethylene glycol (Mg + EG). In another aliquot, the samples were saturated with K and then heated to 500 °C. Slides of oriented clay were prepared for X-ray diffraction (XRD) using a Rigaku Miniflex II device, with Cu (CuKα) radiation, a graphite monochromator, operated at 10 mA and 15 kV, at a rate of 0.02 ° 2θ and a speed of 1 sec/step, in the range of 3 to 45 ° 2θ.

Furthermore, in samples from the A and B horizons from all profiles (P1: A_6, B_1, B_2; P2: A4, B_1, B_3; P3: A_5, AB, B_2; P4: A_3, B_1 and B_3) the Fe-oxyhydroxides in the clay fraction were concentrated with 5 mol L^{-1} NaOH, removing clay minerals and Al-hydroxides (Norrish and Taylor, 1961). Sodium metasilicate was added to reach 0.2 mol L^{-1} Si concentration in solution to avoid the formation of iron oxides with high Al isomorphic substitution (Kämpf and Schwertmann, 1982). Sodalite $[Na_4Al_3Si_3O_{12}(OH)]$ formed during extraction was removed by washing twice with 50 mL of 0.5 mol L^{-1} HCl solution and washing once with 50 mL of deionized water (Norrish and Taylor, 1961; Singh and Gilkes, 1991). The mineral components of the concentrated Fe residue were identified by XRD, carried out on un-oriented powdered samples on glass slides, using a scanning range of 3 to 45 ° 2θ. An internal standard was added to the samples (5 % NaCl) for correction of distortions and mounted on glass slides (non-oriented).

Table 1 – Morphology of the studied soil profiles.

Profile	Hz.	Depth	Color[1]	Structure[2]	Consistency[3]			Waxiness[4]	Coatings surfaces[5]
					Dry	Moist	Wet		
		cm							
P1	A_1	0–10	7.5YR 3/2	SB/G	SO	FR	PL/ST	NO	NO
	A_2	10–20	7.5YR 3/2	SB/G	SO	VFR	PL/ST	NO	NO
	A_3	20–40	7.5YR 3/2	SB/G	SO	VFR	PL/ST	NO	MAS
	A_4	40–65	7.5YR 4/4	SB/G	SO	VFR	PL/ST	NO	MAS
	A_5	65–70	5YR 3/2	SB/G	SO	VFR	PL/ST	NO	MAS
	A_6	70–85	5YR 3/2	SB/G	SO	VFR	PL/ST	NO	MAS
	A_7	85–95	5YR 3/2	SB/G	SO	VFR	PL/ST	NO	MAS
	AB	95–100	5YR 3/3	SB	SO	VFR	PL/ST	NO	MAS
	BA	100–110	5YR 4/4	SB	HA	FR	VPL/VST	SA	SAS
	B_1	110–130	5YR 4/6	SB	HA	FR	VPL/VST	SA	SAS
	B_2	130–170	2.5YR 4/6	SB	HA	VFR	VPL/VST	SA	SAS
	BC	170–200+	5YR 4/6	SB	HA	VFR	VPL/VST	NO	SAS
P2	A_1	0–13	7.5YR 3/2	SB/G	SO	FR	PL/ST	NO	NO
	A_2	13–26	7.5YR 3/2	SB/G	SO	VFR	PL/ST	NO	NO
	A_3	26–70	7.5YR 3/2	SB/G	SO	VFR	PL/ST	NO	NO
	A_4	70–105	7.5YR 2.5/1	SB/G	SO	VFR	PL/ST	NO	NO
	AB	105–120	7.5YR 3/2	SB	SO	VFR	PL/ST	NO	NO
	BA	120–135	7.5YR 3/4	SB	HA	FR	VPL/VST	SA	SAS
	B_1	135–180	7.5YR 4/6	SB	HA	FR	VPL/VST	SA	SAS
	B_2	180–210	5YR 4/6	SB	HA	FR	VPL/VST	SA	SAS
	B_3	210–250	2.5YR 4/6	SB	HA	VFR	VPL/VST	SA	SAS
	B_4	250–320	2.5YR 4/8	SB	EHA	VFR	VPL/VST	SA	SAS
	$2B_5$	320–380	2.5YR 4/6	SB	EHA	VFR	VPL/VST	SA	SAS
	2BC	380–450+	5YR 6/8	SB	SO	VFR	VPL/VST	NO	NO
P3	A_1	0–10	7.5YR 3/2	SB/G	SO	FR	PL/ST	NO	NO
	A_2	10–42	7.5YR 3/2	SB/G	SO	VFR	PL/ST	NO	NO
	A_3	42–60	7.5YR 3/2	SB/G	SO	VFR	PL/ST	NO	NO
	A_4	60–75	7.5YR 3/2	SB/G	SO	VFR	PL/ST	NO	NO
	A_5	75–94	7.5YR 2.5/1	SB/G	SO	VFR	PL/ST	NO	NO
	A_6	94–101	7.5YR 3/2	SB	SO	FR	PL/ST	SA	MAS
	AB	101–118	5YR 3/2	SB	HA	FI	PL/ST	SA	SAS
	BA	118–135	5YR 5/6	SB	HA	FR	VPL/VST	SA	SAS
	B_1	135–165	2.5YR 4/6	SB	HA	VFR	VPL/VST	SA	SAS
	B_2	165–200+	2.5YR 3/6	SB	HA	FR	VPL/VST	SA	SAS
P4	A_1	0–20	7.5YR 3/2	G	SO	VFR	PL/ST	NO	NO
	A_2	20–50	7.5YR 2.5/1	G	SO	VFR	PL/ST	NO	NO
	A_3	50–60	7.5YR 2.5/1	SB	SO	VFR	PL/ST	SC	MAS
	AB	60–65	7.5YR 3/2	SB	HA	VFR	PL/ST	SC	MAS
	BA	65–75	7.5YR 3/2	SB	HA	VFR	VPL/VST	SC	SAS
	B_1	75–110	7.5YR 4/4	SB/P	HA	FR	VPL/VST	SA	SAS
	B_2	110–140	7.5YR 4/6	SB/P	HA	FR	VPL/VST	SA	SAS
	B_3	140–180+	5YR 4/6	SB/P	HA	FR	VPL/VST	SA	SAS

[1]Munsell Color, from Chiapini et al. (2018); [2]Structure: SB = subangular block, G = granular, P = prismatic; [3]Consistency: SO = soft, HA = hard, EHA = extremely hard, FR = friable, VFR = very friable, PL = plastic, ST = sticky, VPL = very plastic, VST = very sticky; [4]Waxiness described in the field: NO = not observed; SC = strong and common; SA = strong and abundant; [5]Coatings surfaces described in the field: NO = not observed; MAS = matte aggregate surface; SAS = shiny aggregate surface. The sombric-like horizon is indicated by grey bands.

The goethite/hematite ratio [Gt/(Gt + Hm)] was estimated using the main diffraction peak areas (Torrent and Cabedo, 1986). Fe isomorphic substitution by Al (IS) in Gt was calculated according to Schulze (1984) and in Hm according to Schwertmann et al. (1979). The Gt and Hm contents were estimated based on the crystalline Fe content (Fe_{CBD} - Fe_o), considering the Gt/(Gt+Hm) ratio, the IS level, and the least mineral formulas (Melo et al., 2001) (Table 5).

Micromorphological analysis

Thin sections (5 × 9 cm) were obtained from Chiapini et al. (2018), and additional data were presented in relation to pedogenetic processes to assist in soil

Table 2 – Granulometry of the studied soil profiles.

Profile	Hz.	Depth	Clay[1]	Silt	Sand[2] Total	VC	C	M	F	VF	Silt/Clay[1]
		cm						g kg⁻¹			
P1	A_1	0–10	530	183	287	27	54	78	98	29	0.4
	A_2	10–20	527	159	314	27	71	87	91	38	0.3
	A_3	20–40	527	167	306	29	61	83	102	31	0.3
	A_4	40–65	552	123	325	30	60	89	112	35	0.2
	A_5	65–70	556	121	323	39	67	96	98	24	0.2
	A_6	70–85	494	209	297	32	62	95	101	8	0.4
	A_7	85–95	510	131	359	41	59	99	125	34	0.3
	AB	95–100	535	124	341	43	58	88	116	35	0.2
	BA	100–110	567	135	298	22	52	83	106	34	0.2
	B_1	110–130	541	169	290	22	58	0	98	33	0.3
	B_2	130–170	426	232	343	29	67	90	105	51	0.5
	BC	170–200⁺	303	382	315	9	47	81	118	60	1.3
P2	A_1	0–13	543	124	333	43	65	89	102	34	0.2
	A_2	13–26	562	135	303	29	55	83	103	33	0.2
	A_3	26–70	587	98	315	27	66	90	99	34	0.2
	A_4	70–105	595	65	340	21	81	100	104	34	0.1
	AB	105–120	597	96	307	27	58	84	104	34	0.2
	BA	120–135	620	62	318	29	61	88	129	11	0.1
	B_1	135–180	652	37	311	34	64	85	95	33	0.1
	B_2	180–210	657	43	301	31	62	81	95	33	0.1
	B_3	210–250	641	49	310	31	68	83	95	33	0.1
	B_4	250–320	634	60	306	42	56	77	100	32	0.1
	$2B_5$	320–380	428	324	248	14	34	54	85	61	0.8
	2BC	380–450⁺	276	407	317	8	23	47	120	119	1.5
P3	A_1	0–10	373	298	329	18	82	98	99	33	0.8
	A_2	10–42	520	170	311	17	66	90	101	36	0.3
	A_3	42–60	542	150	308	22	67	89	98	32	0.3
	A_4	60–75	546	124	330	22	68	93	103	44	0.2
	A_5	75–94	577	103	321	25	61	88	109	38	0.2
	A_6	94–101	576	99	325	32	60	89	104	41	0.2
	AB	101–118	583	95	322	26	60	88	102	45	0.2
	BA	118–135	606	85	309	28	55	79	100	47	0.1
	B_1	135–165	620	99	282	19	55	81	93	33	0.2
	B_2	165–200⁺	654	70	276	22	54	77	90	34	0.1
P4	A_1	0–20	531	188	281	21	51	92	109	8	0.4
	A_2	20–50	505	222	274	21	52	85	111	5	0.4
	A_3	50–60	581	125	294	40	55	83	109	7	0.2
	AB	60–65	556	171	273	32	49	89	102	1	0.3
	BA	65–75	581	141	278	24	48	86	110	10	0.2
	B_1	75–110	586	97	317	15	52	100	111	38	0.2
	B_2	110–140	669	61	271	17	45	78	97	34	0.1
	B_3	140–180⁺	691	62	248	18	43	68	86	32	0.1

[1]From Chiapini et al. (2018); [2]Sand: VC = very coarse; C = coarse; M = medium; F = fine; VF = very fine. The sombric-like horizon is indicated by grey bands.

classification (Table 6 and Figures 3, 4 and 5); these processes included clay illuviation, soil aggregation and, in particular, xanthization.

Results and Discussion

Soil morphology and micromorphology
Surface horizons have a yellowish color, with 7.5 YR hues, which suggests the predominance of goethite rather than hematite (Tables 1 and 5). The darker color observed in sombric-like horizons compared to overlying horizons is related to a larger contribution from BC in the sombric-like horizons (Chiapini et al., 2018), which has a strong pigmentation effect on the soil matrix (Silva and Vidal-Torrado, 1999; Macedo et al., 2017). Thus, the concentration of both BC and OM influence

Table 3 – Chemical properties of the studied soil profiles.

Profile	Hz.	Depth	pH[1] H_2O	H+Al	Al^{3+}	CEC[1]	BS[1]	C_t[1]	C/N	Clay activity[1,2]
		cm		——————— cmolc kg^{-1} ———————			———— % ————			
P1	A_1	0–10	3.8	10.6	5.6	12.1	12	4.9	17	23
	A_2	10–20	3.9	8.0	4.5	8.8	9	4.3	14	17
	A_3	20–40	4.2	7.8	4.2	8.1	3	2.9	14	15
	A_4	40–65	4.5	6.1	3.2	6.6	7	2.9	16	12
	A_5	65–70	4.6	6.3	3.1	6.3	0	2.3	20	11
	A_6	70–85	4.7	6.4	3.0	6.8	5	1.8	21	14
	A_7	85–95	4.7	5.7	2.9	5.7	0	1.3	18	11
	AB	95–100	4.8	5.0	2.7	5.4	8	1.1	16	10
	BA	100–110	4.8	4.4	2.6	4.8	9	0.8	16	8
	B_1	110–130	5.0	3.3	1.9	4.1	20		14	8
	B_2	130–170	5.0	3.0	2.3	3.7	19		13	9
	BC	170–200+	5.1	3.4	3.2	3.9	12			13
P2	A_1	0–13	4.2	8.7	4.2	10.1	14	6.1	15	19
	A_2	13–26	4.0	8.5	3.9	9.2	8	4.8	14	16
	A_3	26–70	4.3	7.8	3.5	8.2	5	4.0	19	14
	A_4	70–105	4.3	7.7	3.3	8.0	4	2.8	22	13
	AB	105–120	4.3	6.5	3.3	6.8	4	2.0	21	11
	BA	120–135	4.4	6.1	2.9	6.6	8	1.7	19	11
	B_1	135–180	4.5	4.4	2.4	4.8	9		15	7
	B_2	180–210	4.8	3.4	1.8	3.8	9		12	6
	B_3	210–250	4.9	3.1	1.2	3.4	10			5
	B_4	250–320	4.7	2.6	1.1	2.9	10			5
	$2B_5$	320–380	4.6	3.5	3.2	4.1	15			9
	2BC	380–450+	4.6	3.6	4.2	4.1	12			15
P3	A_1	0–10	3.9	14.0	5.2	16.7	16	10.3	16	45
	A_2	10–42	4.1	10.1	5.0	11.0	9	7.0	17	21
	A_3	42–60	5.1	7.6	2.4	8.8	13	4.6	15	16
	A_4	60–75	4.5	7.0	3.2	7.1	1	3.3	19	13
	A_5	75–94	4.6	6.6	3.2	6.7	1	3.2	22	12
	A_6	94–101	4.6	6.2	3.3	6.2	1	2.4	22	11
	AB	101–118	4.8	5.3	2.6	5.9	9	1.6	19	10
	BA	118–135	4.8	4.6	2.4	4.6	1	1.4	18	8
	B_1	135–165	4.8	3.7	1.9	3.7	0		13	6
	B_2	165–200+	4.7	3.5	1.6	3.5	0		13	5
P4	A_1	0–20	4.6	9.1	3.1	9.5	4	4.8	19	18
	A_2	20–50	4.9	7.6	2.7	7.7	2	3.7	26	15
	A_3	50–60	5.1	6.2	2.4	6.5	4	2.3	25	11
	AB	60–65	5.0	5.4	2.0	5.8	7	2.7	33	10
	BA	65–75	5.1	4.5	1.5	4.8	8	1.2	21	8
	B_1	75–110	4.9	2.6	0.5	2.6	1		26	4
	B_2	110–140	5.4	2.0	0.3	2.1	1		17	3
	B_3	140–180+	5.4	2.2	0.1	2.2	1			3

[1]From Chiapini et al. (2018); [2]Calculated by: (T value × 1000)/(clay content (g kg^{-1})); The sombric-like horizon is indicated by grey bands.

the melanization process in the upper part of the soil profiles (Macedo et al., 2017).

Field (Table 1) and micromorphological (Table 6) descriptions showed that the soil structure of the surface horizons and sombric-like ones are characterized by granular and subangular blocks with a moderate to strong degree of pedality. This is a result of the high OM content (Table 3; C_t) and an intense bioturbation process (Figure 4 and 5) (De Craene and Laruelle, 1955; Bennema et al., 1970; Macedo et al., 2017). On the other hand, the structure in the subsurface horizons was characterized by subangular blocks with strong pedality indicating a much denser structure (Figure 5). This higher density was related to lower OM content, lower contribution from roots, lower faunal activity, and higher clay content at depth. Shiny and matte aggregate faces were observed in the field (Table 1). On the micro scale, a porostriated b-fabric's features were described and are the result of swell-shrinking of soil in alternating dry and humid periods (Figure 3A, 3B, 3C and 3D).

Table 4 – Iron oxides dissolution of the studied soils.

Profile	Hz.	Depth	Fe_d	Fe_o	Fe_p	Fe_o/Fe_d	Fe_p/Fe_d	Al_d	Al_o	Al_p
		cm	mg kg⁻¹				mg kg⁻¹			
P1	A_1	0–10	48860	4538	20150	0.093	0.412	54650	3520	1701
	A_2	10–20	50650	5750	27670	0.114	0.546	19538	4832	1585
	A_3	20–40	53880	4670	14220	0.087	0.264	32868	4762	1543
	A_4	40–65	52372	4470	18790	0.085	0.359	19488	5182	1979
	A_5	65–70	51860	4278	24990	0.082	0.482	34680	5340	2446
	A_6	70–85	57755	4590	28840	0.079	0.499	27478	5902	2356
	A_7	85–95	63355	3275	19010	0.052	0.3	19018	5182	1914
	AB	95–100	68573	2285	13960	0.033	0.204	24373	4987	1344
	BA	100–110	71371	1537	8380	0.022	0.117	24710	4810	972
	B_1	110–130	72163	1139	450	0.016	0.006	15065	4605	244
	B_2	130–170	77894	1107	36	0.014	0	8765	4075	176
	BC	170–200⁺	77894	666	64	0.009	0.001	19123	3867	223
P2	A_1	0–13	49500	5320	20550	0.107	0.415	40135	5765	4583
	A_2	13–26	55280	5350	25610	0.097	0.463	26720	5660	3576
	A_3	26–70	49595	6355	31100	0.128	0.627	18005	6455	2758
	A_4	70–105	59410	6820	38750	0.115	0.652	8735	7135	638
	AB	105–120	59665	7225	60070	0.121	1.007	44490	6740	4578
	BA	120–135	57285	8055	290	0.141	0.005	25235	6735	804
	B_1	135–180	64466	2214	487	0.034	0.008	8013	5187	311
	B_2	180–210	71529	1691	0	0.024	0	19618	4492	321
	B_3	210–250	75004	1796	0	0.024	0	12818	4442	364
	B_4	250–320	80277	1833	15	0.023	0	3381	4040	148
	$2B_5$	320–380	91530	980	11	0.011	0	7868	3712	213
	2BC	380–450⁺	56382	778	30	0.014	0.001	26768	3742	254
P3	A_1	0–10	40745	4975	17530	0.122	0.43	34353	5677	2607
	A_2	10–42	47022	6898	19640	0.147	0.418	5508	5912	2878
	A_3	42–60	52535	7485	21710	0.142	0.413	3674	6217	3028
	A_4	60–75	52465	5965	17850	0.114	0.34	22353	5957	3818
	A_5	75–94	55615	6975	23190	0.125	0.417	15510	6100	3931
	A_6	94–101	55002	4958	23000	0.09	0.418	12838	4512	2731
	AB	101–118	58282	4098	5660	0.07	0.097	12103	5067	2035
	BA	118–135	57762	2208	780	0.038	0.014	5614	4135	1311
	B_1	135–165	60235	1685	437	0.028	0.007	20573	4337	621
	B_2	165–200⁺	64052	2168	36	0.034	0.001	23273	4557	455
P4	A_1	0–20	63097	9313	39940	0.148	0.633	17138	7192	3996
	A_2	20–50	66667	7753	47460	0.116	0.712	5520	7340	3639
	A_3	50–60	70432	6488	37050	0.092	0.526	10363	6337	3553
	AB	60–65	70697	7403	37930	0.105	0.537	1972	6450	3274
	BA	65–75	70607	7283	33680	0.103	0.477	7018	6632	3730
	B_1	75–110	84902	2148	397	0.025	0.005	16843	4347	672
	B_2	110–140	97685	2205	18830	0.023	0.193	16762	6568	455
	B_3	140–180⁺	97665	3435	13560	0.035	0.139	28630	4630	453

The sombric-like horizon is indicated by grey bands.

Thus, both the shiny and matte surfaces described in the field are actually in fact compression features (shrinking and swelling process) and are not due to clay illuviation.

Thin sections showed a variegated color (red/yellow) in the matrix of B horizons, which were not observed on the macro scale (Figure 3E e 3F). This variegated color is due to xanthization in the A, AB and upper B horizons (Cornell and Schwertmann, 2003). The Gt/(Gt + Hm) ratio would reflect this process, its values varying between 0.423 and 0.754 and indeed indicate predominance of Gt over Hm in the surface horizons of all profiles (Table 5). In fact, the Gt/(Gt + Hm) ratio decreased with depth, indicating xanthization (yellow colors; hues 5 YR and more yellow) in the upper part of the soils (Table 5). The high organic matter content and/or microbial oxidation in the sombric-like horizon inhibits hematite formation at the point of contact with the B horizon, causing preferential reductive dissolution of originally formed hematite turning red soils yellow in the lower subdivisions of the A horizon (Cornell and

Table 5 – Iron oxides quantification of some studied horizons.

	Hz.	WHH+ Gt₁₁₁	Corrected *d*-spacing				Gt/ (Gt+Hm)	MCD#				IS*		Hm	Gt
			Gt_{110}	Gt_{111}	Hm_{104}	Hm_{110}		Gt_{110}	Gt_{111}	Hm_{104}	Hm_{110}	IS_{Gt}	IS_{Hm}		
		(° 2θ)	———————— nm ————————					———————————— nm ————————————				———— % ————			
P1	A_6	1.10	4.15	2.43	2.67	2.51	0.69	21.77	8.92	22.34	18.85	18.01	11.84	2.85	6.35
	B_1	0.97	4.16	2.43	2.69	2.51	0.76	10.05	10.59	20.86	18.50	21.29	13.10	3.05	9.70
	B_2	0.66	4.17	2.44	2.70	2.51	0.56	12.29	18.95	9.40	9.07	14.09	7.14	5.57	7.01
P2	A_4	0.91	4.13	2.42	2.67	2.48	0.84	12.98	11.53	19.55	23.41	23.79	-	1.66	8.70
	B_1	1.01	4.15	2.43	2.75	2.47	0.78	11.59	9.99	13.94	14.09	19.64	-	2.79	9.99
	B_3	0.86	4.15	2.44	2.69	2.47	0.62	20.34	12.65	23.23	24.34	9.86	-	5.52	8.84
P3	A_5	1.03	4.16	2.42	2.66	2.50	0.90	8.03	9.80	20.88	26.41	27.35	-	0.97	8.62
	AB	-	4.13	2.41	2.67	2.51	-	-	-	-	-	32.38	8.90		
	B_2	1.03	4.18	2.43	2.70	2.52	0.56	14.05	9.72	24.86	10.47	18.70	1.32	4.50	5.63
P4	A_3	1.06	4.17	2.44	2.68	2.47	0.85	7.74	9.40	15.40	31.30	9.24	-	1.70	9.75
	B_1	1.37	4.15	2.42	2.66	2.50	0.87	12.21	6.80	15.63	31.91	30.41	-	2.09	14.56
	B_3	1.03	4.18	2.43	2.70	2.51	0.62	14.05	9.72	13.20	11.39	16.53	10.92	6.08	9.89

+ = width at half peak height; # = mean crystal diameter; * = isomorphic substitution. The gray bands are sombric-like horizons.

Table 6 – Micromorphological characteristics of the studied soils.

	Profile P1 - $A_4/A_5/A_6$	Profile P2 - A_4	Profile P3 - A_5/A_6	Profile P4 - A_2
Microstructure	Subangular blocky and granular	Granular	Subangular blocky and granular	Subangular blocky and microgranular
Coarse material	Quartz (95 %); Iron nodules (2 %); Charcoal (3 %)	Quartz (95 %); Iron nodules (2 %); Charcoal (2 %); Mica (< 1 %)	Quartz (96 %); Iron nodules (2 %); Charcoal (2 %)	Quartz (95 %); Iron nodules (3 %); Charcoal (2 %)
Micromass	Speckled, Porostriated	Speckled	Speckled, Pore and Grain Striated	Speckled, Pore and Grain Striated
c/f related distribution	Porfiric-Enaulic	Enaulic-Porfiric	Enaulic-Porfiric	Enaulic-Porfiric
Pedofeatures	Excrement infillings, Incomplete infillings and iron nodules	Incomplete infillings and iron nodules	Excrement infillings, Incomplete infillings and iron nodules	Incomplete infillings and iron nodules

Schwertmann, 2003). Furthermore, the formation of Gt in soils is favored by wetter conditions (Schwertmann and Taylor, 1989), high OM content, low temperature and low contents of Fe in solution (Camêlo et al., 2018), all of which are evident in the soils from the study area.

Chemical and physical properties

The pH in water of the studied soil profiles ranged from 3.8 to 5.4 and increased with depth (Table 3). Extractable aluminum contents (Al^{3+}) in the surface horizons of profiles P1, P2 and P3 were high enough (> 4 $cmol_c$ kg^{-1}) for an aluminic qualifier (Embrapa, 2018); however, in the subsurface horizons this was not observed. Bases (K^+, Na^+, Ca^{2+}, and Mg^{2+} data not shown) and base saturation (BS) were low in all horizons, due to a significant contribution of H + Al ions, as well as low clay activity, which are typical for such highly weathered soils. Similar to Dalmolin et al. (2006), we observed that high Cation Exchange Capacity (CEC) values in the A horizons were a result of the high OM content (C_t; Table 3).

The contents of Fe and Al forms are given in Table 4. The Fe_d contents showed a clear gradual increase with depth, while the opposite was observed for Fe_o (r^2 = 0.93, 0.44, 0.36 and 0.84 for profiles P1–P4,

respectively). This reflects that low OM content favors pedogenic Fe oxyhydroxides formation at depth (mainly hematite) (Curi and Franzmeier, 1987). The Fe_o/Fe_d ratio showed generally higher values in the A than in the B horizons because of the high influence of OM in the A horizons (Table 4). The Fe_o/Fe_d ratio indicated that the Fe in the A horizons was in poorly ordered form (values > 0.05), while in the B horizons the major part of Fe oxides were present in crystals with greater ordered form (values < 0.05; Inda Junior and Kämpf, 2003). The Fe_p was substantially higher than the Al_p, and both showed positive correlation (r^2 = 0.76). The high values of Fe_p and of the Fe_p/Fe_d ratio indicate that Fe is bound to soil OM and confirms that part is in the non-crystalline form.

High Al_d values were observed in surficial horizons, which can be related to several methodological factors during the sodium citrate-bicarbonate-dithionite (CBD) extractions. First, successive extractions with CBD (80 °C) may dissolve a certain amount of kaolinite and gibbsite thereby releasing Al^{3+} and causing an increase in Al_d (Inda Junior and Kämpf, 2003). Second, the high Al_d values can be due to complexation to sodium citrate catalyzed by the high temperature during the extraction procedure (Zhang et al., 1985). Third, the high values of
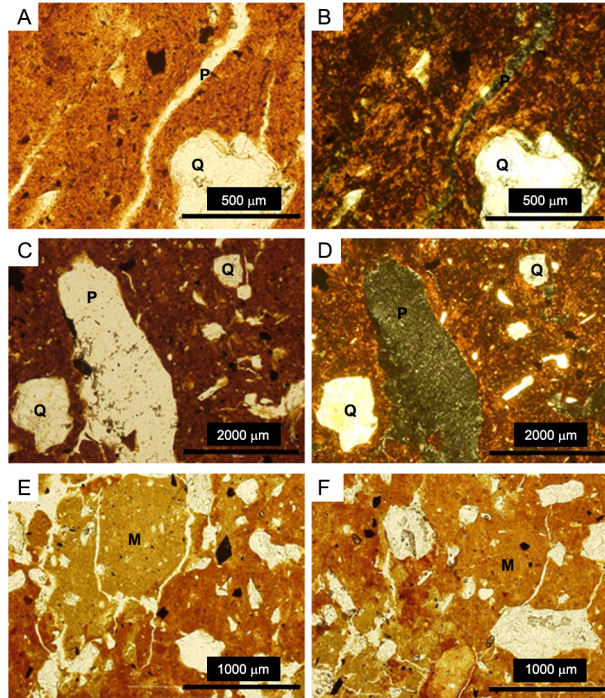
Figure 3 – Photomicrographs. A), D) (polarized light), B) and D) (cross polarized light) Porostriated b fabric (shiny peds) due to moderate shrinking and swelling of aggregates in B horizon of P1; E) and F) Soil matrix in B horizon (variegated color) and microscopic fragments of charcoal of P2, representing the xanthization process below the 'sombric' horizon (sombric-like horizon). Q: quartz; P: pore and M: soil matrix.
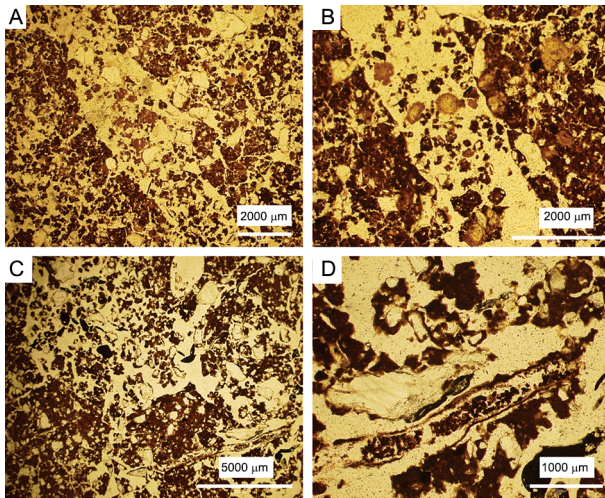

Figure 5 – Increase in structure density with depth. A) and B) Subsurface horizon with subangular block and granular structure (P3 transition A3/A4; 57–72 cm); C), D) and E) Subsurface horizon with subangular block structure (P3 transition A5/A6; 77–90 cm); F) Subsurface horizon with subangular block structure (P3 horizon B2; 170–183 cm).

Figure 4 – The bioturbation process. A) and B) Loose discontinuous infillings in the A4 horizon of P2 and the granular structure; C) Loose discontinuous infillings in the A5 horizon of P3; D) Detail of C).

Al_d can be related to the extraction of the Al^{3+} resulting from the isomorphic substitution of Fe^{3+} in the iron oxides (Tables 4 and 5).

All four profiles presented a high clay content that was regularly distributed with depth (Table 2). The highest clay contents were observed in B horizons but this was not sufficient to characterize a textural difference (clay increase in depth) (IUSS Working Group WRB, 2015; Soil Survey Staff, 2014; Embrapa, 2018). The B horizons presented a low silt/clay ratio (~ 0.3), which is typical of highly weathered soils (Fox, 1982) where the clay content increases due to weathering of minerals in the silt fraction. Thus, properties such as low activity clays, silt/clay and Feo/Fed ratios characterizes the occurrence of a moderate ferralitization process in our studied soils (Kämpf and Curi, 2012).

Clay mineralogy

Clay components identified with XRD in the iron-free clay fraction of B horizons of all profiles were kaolinite (Kt), gibbsite (Gb), hydroxy-interlayered 2:1 minerals (2:1 HI) and quartz (Qz) (Figure 6). The intensities of Kt_{001} and Gb_{002} decreased from the profile at the summit (P1) towards the profile at the footslope (P3). 2:1 HI showed similar intensities in profiles P1 and P2, but was very weak in profiles P3 and P4. The absence of significant asymmetry of Kt_{001} in profiles P1 and P2 indicates no or little interstratification with smectite,
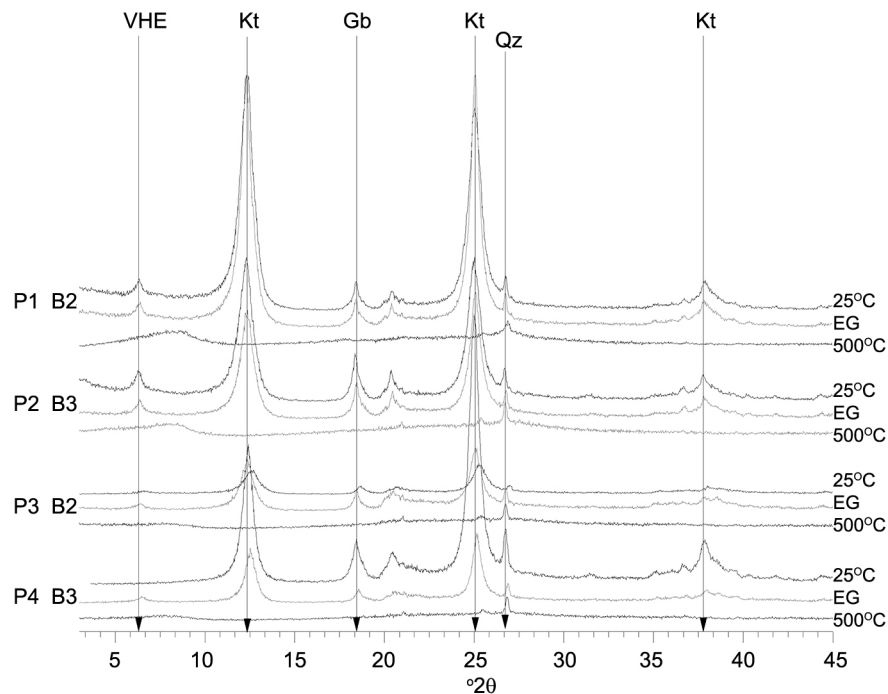
Figure 6 – Diffractograms of the clay content of the B horizons, saturated with Mg (Mg 25 °C), solvated with ethylene glycol (Mg + EG) and K heated until 500 °C (500 °C). All profiles (P1, P2, P3 and P4), there is the presence of kaolinite (Kt), gibbsite (Gb), 2:1 hydroxy-interlayered (HI) and quartz (Qz).

which is in agreement with observations on similar soils in the region by Oliveira Junior et al. (2014).

Goethite and hematite were identified in the concentrated oxide fraction (Figure 7). The contents of goethite varied from 5 % to 11 % and that of hematite from 2 % to 7 %. Goethite predominated in all studied soil profiles, with the exception of the B₃ and B₂ horizons from P2 and P3, respectively (Table 5). The data showed the highest goethite content in soil profiles was in the first B horizon (B1) (Table 5). The yellow color was observed reflecting the morphology of xanthization (Figures 3E – 3F) which occurs in the interface of the sombric-like horizon that is rich in OM (Cₜ) and the B horizon; and the action of soil fauna in this interface aid which is responsible for the distribution of OM in depth (melanization), that consequently expands xanthization. According to Chiapini et al. (2018), the sombric-like horizon of these soils is a remnant of an earlier phase of soil formation under grass vegetation and frequent natural fires resulting in considerable accumulation of black carbon (BC) at depth. During wetter conditions, from the Late Holocene period to the present, xanthization was influenced by this accumulation of OM and contributed to the development of polychrome of soil profiles.

The Hm content showed a clear increase with depth, which was the reverse for Gt (Almeida et al., 2000). The values for isomorphic substitution (IS) varied from 9 % to 32 % for Gt and from 1 % to 11 % for Hm. The IS for Gt presented similar values in both the A and upper B horizons for all profiles, with the exception of profile P2 where the A horizon presented a higher IS value (Table 5). This high Al goethite substitution is related to elevated, dessicated non-hydromorphic conditions that were observed in our soil profiles similar to other highly weathered Brazilian soils (Schwertamenn and Kämpf, 1985; Motta and Kämpf, 1992; Almeida et al., 2000). The deepest horizon showed lower IS values for both Gt and Hm (Table 5). In P2 and certain horizons of P3 (A5) and P4 (A3 and B1) it was not possible to obtain IS values for Hm.

The mean crystal diameter (MCD) of Gt showed a similar growth tendency for both directions (110 and 111), with the exception of the B₃ horizon from profile P2. In Hm, the crystals showed a tendency to grow in a 104 rather than a 110 direction, again with exception of the B₃ horizon from profile P2, in which similar dimensions for both directions were observed. The MCD for Gt and Hm in the studied profiles was smaller than that observed by Melo et al. (2001) in tropical conditions (hot and humid). Furthermore, the size of Hm and Gt crystals was smaller (< 5 nm; Table 5) than that observed in Oxisols (Melo et al., 2001; Lima et al., 2017). Thus, high Kt content favors the development of a block structure rather than a granular microstructure in the B horizons (De Wispelaere et al., 2015). No evidence of coalescence of microstructures nor transformation from small granular to blocky or prismatic aggregates were observed, as was proposed by Cooper et al. (2010).
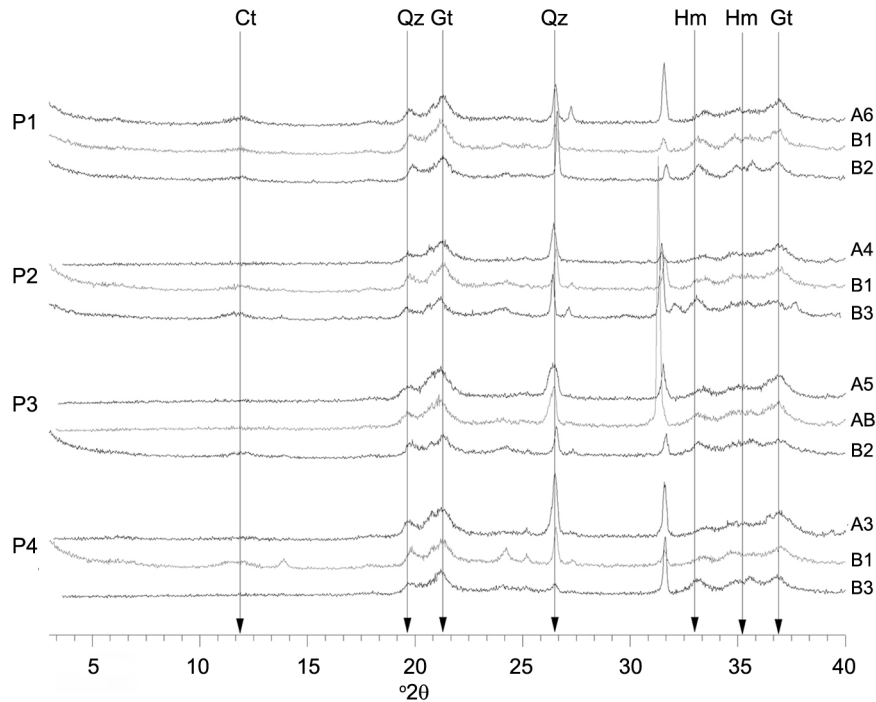
Figure 7 – Diffractograms after concentration of iron oxides in some soil horizons.

Soil Classification

Important items for classification at the Order level are the morphological features related to the B horizon. These include particle rearrangement on the surfaces of structural units, shiny peds, low textural difference, clay-rich subsoil and structure from moderate to strong subangular blocks with waxiness characterizing a *Nítico* and *Textural* horizon at the same time as according to the Brazilian Soil Classification System (Embrapa, 2018). At WRB-FAO (IUSS Working Group, 2015) the B horizon is classified as a Nitic horizon, presenting the same morphological features and chemical characteristics such as ≥ 4 % Fed and ≥ 0.2 % Feo. In relation to Soil Taxonomy (Soil Survey Staff, 2014) the B horizon is classified as a Kandic horizon.

Another important classification item is the polychrome character of the soil profiles. As per the Brazilian Soil Classification System (Embrapa, 2018), in the *Nitossolos* Order (*Nítico* B horizon), the polychrome indication is only allowed in specific situations, none of which fit in our soils. The soil profiles showed colors of more than one hue page, and variation in value and chroma in A and B horizons (Table 1). Similarly, in the suborder, *Nitossolos Brunos*, this variation in color is also not allowed. Because of this, the profiles must be classified as *Argissolos* in the first Order.

Classification of the four soil profiles (P1–P4) under the Brazilian Soil Classification System (Embrapa, 2018) would result in the following reasoning:

Due to the presence of the *Nítico* and *Textural* B horizon with shiny peds that cannot be attributed to clay illuviation, nor polychrome characteristic, the first category level (Order) is classified as *Argissolos*. Because the soils presented a red-yellow color (P1), dominant yellow color (P2 and P4) and dominant red color (P3) in the BA and B horizons, they were classified as Vermelho-Amarelo (Red-Yellow) in the second level in P1, Amarelo (Yellow) in the second level of P2 and P4, and Vermelho (Red) in the second level in P3. The soil profiles showed low base saturation (BS < 50 %). Thus the third category level they were classified as Distrófico (Dystrophic). At the fourth category level the soil profiles P1 and P3 were classified as *nitossólico*, because of the soil morphology similar to *Nitossolos* and soil profiles P2 and P4 such as típico (typical) (Table 7). Additional problems with the Brazilian Soil Classification System (Embrapa, 2018) were observed at the subgroup level, where the sombric feature (*caráter sômbrico*) is not allowed because i) no OM illuviation was confirmed in the micromorphological analysis (organic or clay-organic coatings) and ii) no increase in carbon content in the sombric-like horizons was observed. The impossibility of classifying it as a sombric horizon thereby neglects an important process related to its formation, i.e., decomposition of the upper part of a humic horizon (Caner et al., 2003; Chiapini et al., 2018). As such, a great effort dispensed in pedogenic studies that use the soil as a record of past climatic conditions will be missed, as well as one of the main soil forming factors, i.e. time, is neglected.

This situation must be revisited once all of the soil classification systems used in this work have assumed the taxonomic approach, in other words, considered the pedogenic process to fit a soil in a given class.

Table 7 – Soil Classification in the Brazilian Soil Classification System (SiBCS; Embrapa, 2018), WRB (IUSS Working Group WRB, 2015) and Soil Taxonomy (Soil Survey Staff, 2014).

Soil profile	Classification		
	SiBCS	WRB	Soil Taxonomy
P1	ARGISSOLO Vermelho-Amarelo nitossólico	Umbric Nitisol (Dystric, Humic)	Typic Kandiudox
P2	ARGISSOLO Amarelo distrófico típico	Umbric Nitisol (Dystric, Humic)	Xanthic Kandiudox
P3	ARGISSOLO Vermelho distrófico nitossólico	Umbric Nitisol (Rhodic, Dystric, Humic)	Rhodic Kandiudox
P4	ARGISSOLO Amarelo distrófico típico	Umbric Nitisol (Dystric, Humic)	Xanthic Kandiudox

In the WRB classification (IUSS Working Group WRB, 2015), the polychrome characteristic is not a problem and the sombric horizon can be assigned to this soil order, but it cannot appear in principal qualifiers nor in supplementary ones. Therefore, the presence of a sombric horizon or a sombric qualifier could not be identified in the studied soil profiles and their classification in WRB would result in Umbric Nitisol due to the presence of a nitic and umbric horizon. As regards qualifiers, the soils P1, P2 and P4 were classified as Dystric and Humic and P3 as Rhodic, Dystric and Humic (Table 7). Our classification differs from Bockheim (2012) who found the sombric horizons primarily in Umbric Ferralsols (Sombric).

In Soil Taxonomy (Soil Survey Staff, 2014) no problems with morphological characteristics were found and the soils were classified as Oxisol in the Order level because of the low base saturation and high mineral weathering (moderate ferralitization). A Udic moisture regime was identified as the Suborder level. At Great Group the soil profiles were classified as Typic Kandiudox (P1), Xanthic Kandiudox (P2 and P4: dominant yellow color) and Rhodic Kandiudox (P4: dominant red color) (Table 7). Similar to those described above, Bockheim (2012) classified soils with a sombric horizon primarily as Sombriudox and Sombrihumult in Soil Taxonomy, which differs somewhat from our soils.

Thus, the sombric-like horizon in the soils from our study area cannot be classified as sombric horizons according to the Soil Taxonomy and WRB classification systems, nor as a sombric qualifier according to the Brazilian Soil Classification System.

The process of OM illuviation (Soil Survey Staff, 2014; IUSS Working Group WRB, 2015) in the formation of the sombric horizon was not observed in any of our four soil profiles (Figure 3A and 3B). Nevertheless, the other characteristics belonging to the sombric horizon were present, and included base saturation < 50 %, lateral tracing that distinguished them from some buried epipedons, and a lower color value and chroma than the overlying horizon.

Conclusions

The distinctive properties of subtropical soils with sombric-like horizon from the studied soil profiles included: the presence of shiny peds, a base saturation < 50 %, a lower color value and chroma than the overlying horizon, clear and sharp lateral tracing, the yellowish color in depth, and the polychrome characteristic. Melanization, xanthization, bioturbation, moderate shrinking/swelling and moderate ferralitization are the most evident pedogenetic processes. Xanthization is closely related to the formation of the sombric-like horizon during the past change from drier to wetter conditions.

The current definition of the sombric horizon in the soil classification systems (Soil Taxonomy, WRB-FAO and Brazilian Soil Classification) can be improved in terms of soil forming processes and polychrome characteristic. We propose developing classification criteria for the sombric-like horizon, or alternatively accept them as a special type of sombric horizon.

Acknowledgments

Authors' Contributions

Conceptualization: Chiapini, M.; Vidal-Torrado, P.; **Data acquisition:** Chiapini, M.; Oliveira Junior, J.C.; Schellekens, J.; Almeida, J.A.A. **Data analysis:** Chiapini, M.; Vidal-Torrado, P., Oliveira Junior, J.C., Schellekens, J.; Almeida, J.A. **Design of methodolog**y: Chiapini, M.; Vidal-Torrado, P. **Writing and editing:** Chiapini, M.; Schellekens, J.; Vidal-Torrado, P.; Oliveira Junior, J.C.; Almeida, J.A.; Buurman, P.

References

Almeida, J.A.; Maçaneiro, K.C.; Klamt, E. 2000. Clay mineralogy of high altitude red soils with brown or yellowish brown surface horizons. Revista Brasileira de Ciência do Solo 24: 815-828 (in Portuguese, with abstract in English).

Almeida, J.A.; Cararo, D.C.; Uberti, A.A.A. 2009. Genesis of the sombric horizon in Ultisols (Red Argisols) in southern Santa Catarina, Brazil. Revista Brasileira de Ciência do Solo 33: 405–416.

Almeida, J.A.; Lunardi Neto, A.; Vidal-Torrado, P. 2015. Sombric horizon: five decades without evolution: a review. Scientia Agricola 72: 87–95.

Behling, H.; Bauermann, S.G.; Neves, P.C. 2001. Holocene environmental changes from the São Francisco de Paula region, southern Brazil. Journal of South American Earth Science 14: 631–639.

Bennema, J.; Jongerius, A.; Lemos, R. 1970. Micromorphology of some oxic and argillic horizons in south Brazil in relation to weathering sequences. Geoderma 4: 333–355.

Bockheim, J.G. 2012. Revisiting the definitions of the sombric horizon in soil taxonomy and word reference base for soil resources. Geoderma 170: 127–135.

Camêlo, D.L; Ker, J.C.; Fontes, M.P.F.; Costa, A.C.S.; Corrêa, M.M.; Leopold, M. 2018. Mineralogy, magnetic susceptibility and geochemistry of Fe-rich Oxisols developed from several parent materials. Scientia Agricola 75: 410–419.

Caner, L.; Toutain, F.; Bourgeon, G.; Herbillon, A.J. 2003. Occurrence of sombric-like subsurface A horizons in some andic soils of the Nilgiri Hills (southern India) and their palaeoecological significance. Geoderma 117: 251–265.

Chiapini, M.; Schellekens, J.; Calegari, M.R.; Almeida, J.A.; Buurman, P.; Camargo, P.B.; Vidal-Torrado, P. 2018. Formation of black carbon rich 'sombric' horizons in the subsoil: a case study from subtropical Brazil. Geoderma 314: 232–244.

Cooper, M.; Vidal-Torrado, P.; Grimaldi M. 2010. Soil structure transformations from ferralic to nitic horizons on a toposequence in southeastern Brazil. Revista Brasileira de Ciência do Solo 34: 1685–1699.

Cornell, R.M.; Shwertmann, U. 2003. The Iron Oxides: Structure, Properties, Reactions and Uses. Wiley, New York, NY, USA.

Curi, N.; Franzmeier D.P. 1987. Effect of parent rocks on chemical and mineralogical properties of some Oxisols in Brazil. Soil Science Society of America Journal 51:153–158.

Dalmolin, R.S.D.; Gonçalves, C.N.; Dick, D.P.; Knicker, H.; Klamt, E.; Kögel-Knabner, I. 2006. Organic matter characteristics and distribution in Ferralsol profiles of a climosequence in southern Brazil. European Journal of Soil Science 57: 644–654.

De Craene, A.; Laruelle, J. 1955. Genesis and alteration of equatorial and tropic latosols. Bulletin Agricole du Congo Belge 46: 1113–1243 (in French, with abstract in English).

De Wispelaere, L.; Marcelino, V.; Regassa, A.; De Grave, E.; Dumon, M.; Mees, F.; Van Ranst, E. 2015. Revisiting nitic horizon properties of Nitisols in SW Ethiopia. Geoderma 243–244: 69–79.

Empresa Brasileira de Pesquisa Agropecuária [EMBRAPA]. 2018. Brazilian soil classification system. Available at: https://www.embrapa.br/busca-de-publicacoes/-/publicacao/1094001/brazilian-soil-classification-system [Accessed Feb 9, 2019]

Food and Agriculture Organization of the United Nations [FAO]. 2006. Guidelines for Soil Description. 4ed. FAO, Rome, Italy.

Faivre, P. 1990. The sombric horizon: an 'incipient' organic-argillic horizon; the example of soils of the intra-Andean region of Colombia (South America). Pédologie 40: 273–297 (in French, with abstract in English).

Fox, R.L. 1982. Some highly weathered soils of Puerto Rico. 3. Chemical properties. Geoderma 27: 139–176.

Gouveia, S.E.M.; Pessenda, L.C.R.; Aravena, R.; Boulet, R.; Scheel-Ybert, R.; Bendassoli, J.A.; Ribeiro, A.S.; Freitas, H.A. 2002. Carbon isotopes in charcoal and soils in studies of paleovegetation and climate changes during the late Pleistocene and the Holocene in the southeast and center west regions of Brazil. Global and Planetary Change 33: 95–106.

Inda Junior, A.V.; Kämpf, N. 2003. Evaluation of pedogenic iron oxide extraction procedures with sodium dithionite-citrate-bicarbonate. Revista Brasileira de Ciência do Solo 27:1139–1147 (in Portuguese, with abstract in English).

IUSS Working Group WRB. 2015. World Reference Base for Soil Resources 2014: Update 2015. International Soil Classification System for Naming Soils and Creating Legends for Soil Maps. FAO, Rome, Italy. (World Soil Resources Reports, 106).

Jackson, M.L. 1979. Soil Chemical Analysis: Advanced Course; A manual of methods useful for instruction and research in soil chemistry, physical chemistry of soils, soil fertility, and soil genesis. The author, Madison, WI, USA.

Kämpf, N.; Curi, N. 2012. Formation and evolution of soil: pedogenesis = Formação e evolução do solo: pedogênese. p. 207–302. In: Ker, J.C.; Curi, N.; Schaefer, C.E.G.R.; Vidal-Torrado, P, eds. Pedology: elements = Pedologia: fundamentos. Sociedade Brasileira de Ciência do Solo, Viçosa, MG, Brazil (in Portuguese).

Kämpf, N.; Schwertmann, U. 1982. The NaOH concentration method for iron oxides in soils. Clays and Clay Minerals 30: 401–408.

Lebedeva, I.I.; Tonkonogov, V.D.; Gerasimova, M.I. 1999. Diagnostic horizons in substantive-genetic soil classification systems. Eurasian Soil Science 32: 959–965

Lima, D.C.; Ker J.C.; Fontes M.P.F.; Corrêa, M.M.; Costa A.C.S.; Melo V.F. 2017. Pedogenic iron oxides in iron-rich oxisols developed from mafic rocks. Revista Brasileira de Ciência do Solo 41: 1–16.

Macedo, R.S.; Teixeira, W.G.; Corrêa, M.M.; Martins, G.C.; Vidal-Torrado, P. 2017. Pedogenetic processes in anthrosols with pretic horizon (Amazonian Dark Earth) in Central Amazon, Brazil. PloS ONE 12: e0178038.

McKeague, J.A.; Day, J.H. 1966. Dithionite and oxalate-extractable Fe and Al as aids in differentiating various classes of soils. Canadian Journal of Soil Science 46: 13–22.

Mehra, J.P.; Jackson, M.L. 1960. Iron oxides removal from soils and clays by a dithionite-citrate-bicarbonate system buffered with bicarbonate sodium. Clays and Clay Minerals 7: 317–327.

Melo, V.F.; Fontes, M.P.F.; Novais, R.F.; Singh, B.; Schaefer, C.E.G.R. 2001. Iron and aluminum oxides of different Brazilian soils. Revista Brasileira de Ciência do Solo 25: 19–32 (in Portuguese, with abstract in English).

Motta, P.E.F.; Kämpf, N. 1992. Iron oxide properties as support to soil morphological features for prediction of moisture regimes in Oxisols of central Brazil. Journal of Plant Nutrition and Soil 155: 385–390.

Norrish, K.; Taylor, M. 1961. The isomorphous replacement of iron by aluminium in soil goethites. European Journal of Soil Science 12: 294–306.

Oliveira Junior, J.C.; Melo, V.F.; Souza L.C.P.; Rocha, H.O. 2014. Terrain attributes and spatial distribution of soil mineralogical attributes. Geoderma 213: 214–225.

Santos, L.C.; Oka-Fiori, C.; Canali, N.E.; Fiori, A.P.; Silveira, C.T.; Silva, J.M.F.; Ross, J.L.S. 2006. Geomorphological mapping of the state of Paraná. Revista Brasileira de Geomorfologia 2: 3–12 (in Portuguese, with abstract in English).

Silva, A.C.; Vidal-Torrado, P. 1999. Genesis of humic Oxisols and its relationships with the evolution of the landscape of a cratonic area in the south of Minas Gerais state, Brazil. Revista Brasileira de Ciência do Solo 23: 329–341(in Portuguese, with abstract in English).

Schulze, D.G. 1984. The influence of aluminium on iron oxides. VIII. Unit-cell dimen- sions of Al-substituted goethites and estimation of Al from them. Clays and Clay Minerals 32: 36–44.

Schwertmann, U.; Taylor, R.M. 1989. Iron oxides. p. 379–438. In: Dixon, J.B.; Weed, S.B., eds. Minerals in soil environments. 2ed. Soil Science Society of America, Madison, WI, USA.

Schwertmann, U.; Kämpf, N. 1985. Properties of goethite and hematite in kaolinitic soils of southern and central Brazil. Soil Science 139: 344–350.

Schwertmann, U.; Fitzpatrick, R.W.; Taylor, R.M.; Lewis, D.G. 1979. The influence of aluminium on iron oxides. Part II. Preparation and properties of Al-substituted hematites. Clays and Clay Minerals 29: 269–276.

Singh, B.; Gilkes, R.J. 1991. Concentration of iron oxides from soils clays by 5 M NaOH treatment: the complete removal of sodalite and kaolin. Clay Minerals 26: 463–472.

Soil Survey Staff. 2014. Keys to Soil Taxonomy. 12ed. USDA-NRCS, Washington, DC, USA.

Sys, C.; Van Wambecke, A.; Frankart, R.; Gilson, P.; Jongen, P.; Pécrot, A.; Berce, J.M.; Jamagne, M. 1961. Soil Cartography in Congo: Principles and Methods = La Cartographie des Sols au Congo, ses Principes et ses Méthodes. National Institute for Agronomy in Belgian Congo, Brussels, Belgium. (Series Science, 66) (in French).

Torrent, J.; Cabedo, A. 1986. Sources of iron oxides in reddish brown soil profiles from calcarenites in southern Spain. Geoderma 37: 57–66.

United States Department of Agriculture [USDA]. 1996. Soil Survey Laboratory Methods Manual. USDA, Washington, DC, USA.

Velasco-Molina, M.; Almeida, J.A.; Vidal-Torrado, P.; Macías, F. 2010. Chemical fractionation of carbon on Acrisols with sombric horizon from south Brazil. Revista de Ciências Agrárias 33: 277–286 (in Spanish, with abstract in English).

Zhang, Y.; Kallay, N.; Matijevic, E. 1985. Interactions of metals hydrous with chelating agentes. VII. Hematite-oxalic and citric acid systems. Langmuir 1: 201–206.